

## Accepted Manuscript

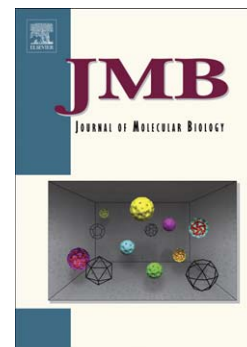
Oligomeric Structure of *Anabaena* Sensory Rhodopsin in a Lipid Bilayer Environment by Combining Solid-State NMR and Long-range DEER Constraints

Sergey Milikisiyants, Shenlin Wang, Rachel A. Munro, Matthew Donohue, Meaghan E. Ward, David Bolton, Leonid S. Brown, Tatyana I. Smirnova, Vladimir Ladizhansky, Alex I. Smirnov

PII: S0022-2836(17)30219-X  
DOI: doi:[10.1016/j.jmb.2017.05.005](https://doi.org/10.1016/j.jmb.2017.05.005)  
Reference: YJMBI 65406

To appear in: *Journal of Molecular Biology*

Received date: 22 March 2017  
Revised date: 27 April 2017  
Accepted date: 6 May 2017



Please cite this article as: Milikisiyants, S., Wang, S., Munro, R.A., Donohue, M., Ward, M.E., Bolton, D., Brown, L.S., Smirnova, T.I., Ladizhansky, V. & Smirnov, A.I., Oligomeric Structure of *Anabaena* Sensory Rhodopsin in a Lipid Bilayer Environment by Combining Solid-State NMR and Long-range DEER Constraints, *Journal of Molecular Biology* (2017), doi:[10.1016/j.jmb.2017.05.005](https://doi.org/10.1016/j.jmb.2017.05.005)

This is a PDF file of an unedited manuscript that has been accepted for publication. As a service to our customers we are providing this early version of the manuscript. The manuscript will undergo copyediting, typesetting, and review of the resulting proof before it is published in its final form. Please note that during the production process errors may be discovered which could affect the content, and all legal disclaimers that apply to the journal pertain.

# **Oligomeric Structure of *Anabaena* Sensory Rhodopsin in a Lipid Bilayer Environment by Combining Solid-State NMR and Long-range DEER**

## **Constraints**

Sergey Milikisiyants<sup>a</sup>, Shenlin Wang<sup>b</sup>, Rachel A. Munro<sup>c</sup>, Matthew Donohue<sup>a,1</sup>, Meaghan E. Ward<sup>c,2</sup>, David Bolton<sup>c</sup>, Leonid S. Brown<sup>c</sup>, Tatyana I. Smirnova<sup>a</sup>, Vladimir Ladizhansky<sup>c\*</sup>, Alex I. Smirnov<sup>a\*</sup>

<sup>a</sup>Department of Chemistry, College of Sciences, 2620 Yarbrough Drive, North Carolina State University, Raleigh, North Carolina, 27695-8204, USA

<sup>b</sup>Beijing Nuclear Magnetic Resonance Center and College of Chemistry and Molecular Engineering, Peking University, 5 Yiheyuan Road, Haidian, Beijing, 100871, People's Republic of China

<sup>c</sup>Department of Physics and Biophysics Interdepartmental Group, University of Guelph, 50 Stone Rd E., Guelph, Ontario, N1G 2W1, Canada

\**Corresponding authors*. E-mail addresses: alex\_smirnov@ncsu.edu, vladizha@uoguelph.ca

<sup>1</sup>Present address: M. Donohue, National Institute of Science and Technology, 100 Bureau Drive, Gaithersburg, MD 20899-6204, United States.

<sup>2</sup>Present address: Meaghan E. Ward, Department of Chemistry, Faculty of Science, Bijvoet Center for Biomolecular Research, Utrecht University, Padualaan 8, 3584 CH Utrecht, The Netherlands

**Key words:** double electron–electron resonance (DEER); site-directed spin labeling; solid-state NMR; paramagnetic relaxation enhancement; membrane protein structure.

**Abbreviations used:** bR, bacteriorhodopsin; DEER, double electron–electron resonance; CW EPR, continuous wave EPR; TM, transmembrane; ASR, *Anabaena* Sensory Rhodopsin; bR, bacteriorhodopsin; SDS, sodium dodecyl sulfate; DMPC, 1,2-dimyristoyl-*sn*-glycero-3-phosphocholine; 7TM, seven-helical transmembrane; cryo-EM, cryo-electron microscopy; FRET, Förster resonance energy transfer; LRET, luminescence resonance energy transfer; MAS ssNMR, magic angle spinning solid-state nuclear magnetic resonance; OS, oriented-sample; SDSL, site-directed spin labeling; pR, proteorhodopsin; NOE, nuclear Overhauser effect; PRE, paramagnetic relaxation enhancement; RMSD, root-mean-square deviation; PDB, protein data bank; SAXS, small angle x-ray scattering; MTSL, (S-(1-oxyl-2,2,5,5-tetramethyl-2,5-dihydro-1H-pyrrol-3-yl)methyl methanesulfonothioate; MD, molecular dynamics; DMPA, 1,2-ditetradecanoyl-*sn*-glycero-3-phosphate; DDM, *n*-dodecyl  $\beta$ -D-maltoside; MMTS, methyl methanethiosulfonate; NCA, N to C $\alpha$  magnetization transfer.

**ABSTRACT**

Oligomerization of membrane proteins is common in nature. Here, we combine spin-labeling Double Electron-Electron Resonance (DEER) and solid-state NMR (ssNMR) spectroscopy to refine the structure of an oligomeric integral membrane protein, *Anabaena* Sensory Rhodopsin (ASR), reconstituted in a lipid environment. An essential feature of such a combined approach is that it provides structural distance restraints spanning a range of *ca.* 3-60 Å, while using the same sample preparation (*i.e.*, mutations, paramagnetic labeling, and reconstitution in lipid bilayers) for both ssNMR and DEER. Direct modelling of the multispin effects on DEER signal allowed for the determination of the oligomeric order and for obtaining long-range DEER distance restraints between the ASR trimer subunits that were used to refine solid-state NMR structure of ASR. The improved structure of the ASR trimer revealed a more compact packing of helices and side chains at the intermonomer interface, compared to the structure determined using the ssNMR data alone. The extent of the refinement is significant when compared with typical helix movements observed for the active states of homologous proteins. Our combined approach of using complementary DEER and NMR measurements for the determination of oligomeric structures would be widely applicable to membrane proteins where paramagnetic tags can be introduced. Such a method could be used to study the effects of the lipid membrane composition on protein oligomerization as well as to observe structural changes in protein oligomers upon drug, substrate, and co-factor binding.

## Introduction

The structure and function of integral membrane proteins are affected by many factors, including physicochemical interactions with other membrane constituents such as lipids and proteins. The protein-protein interactions could occur either transiently or through a formation of more stable oligomeric complexes. Oligomerization is a rather common biophysical phenomenon that is often the final step of protein folding into functional assemblies.<sup>1</sup> Some notable well-studied examples of functional oligomers include both bitopic and polytopic membrane proteins, such as glycophorin A,<sup>2</sup> influenza A M2 H<sup>+</sup> channel,<sup>3</sup> K<sup>+</sup> channels,<sup>4</sup> and several G-protein coupled receptors.<sup>5</sup> Stability of the oligomeric complexes varies widely. For example, a tetrameric SKC1 K<sup>+</sup> channel is known to persist even under highly denaturing conditions that include 8 M urea, 6 M guanidinium chloride, and 2% SDS.<sup>6</sup> Such stable protein oligomers can be readily characterized in the solubilized state using a number of analytical methods: protein electrophoresis, size exclusion chromatography, and analytical centrifugation - to name a few.<sup>7; 8; 9; 10</sup> However, it is not uncommon for the oligomeric structure to be affected by the membrane lipid composition and even sample preparation procedures.

In particular, the type of lipid mimetics and even the chemistry of specific detergents or lipids can affect the protein structure<sup>11</sup> and its oligomeric state.<sup>12</sup> One example is a seven-helical (7TM) protein bacteriorhodopsin (bR) which forms stable trimers in the native purple membrane, but the trimers dissociate upon reconstitution in synthetic lipids at a high lipid-to-protein ratio.<sup>13</sup> An increase in temperature also triggers a dissociation of the bR trimers reconstituted in DMPC (1,2-dimyristoyl-*sn*-glycero-3-phosphocholine) lipid bilayers.<sup>13</sup> Another example is provided by a 7TM protein proteorhodopsin (pR), for which the oligomeric order, populations of the oligomeric states, as well as the proximity of proteins within the oligomers, are all affected by the surfactant type.<sup>14; 15; 16</sup>

Currently, the repertoire of experimental methods suitable for quantitation and structure determination of protein oligomers in the lipid milieu remains limited. For example, cryo-EM and single particle cryo-EM are suitable for studying membrane-anchored<sup>17</sup> and integral membrane proteins.<sup>18</sup> However, reconstruction of the 3D structures to high resolution often relies on fitting the available crystal structures of the individual subunits to the EM data<sup>18</sup> unless high quality 2D crystals of membrane proteins could be obtained. While FRET and LRET, including single-molecule variants of these methods, provide for determination of the oligomeric states of membrane proteins even in living cells,<sup>19</sup> these spectroscopic techniques lack the structural capabilities of x-ray crystallography and NMR in both the number and accuracy of the attainable structural restraints.

In recent years a notable progress in solving structures of membrane proteins has been achieved by solid-state NMR (ssNMR) which does not require protein crystallization.<sup>20; 21; 22; 23,24; 25</sup> NMR structures are derived from a large number of short-range internuclear distance restraints and medium-range paramagnetic ssNMR restraints.<sup>26; 27; 28; 29; 30; 31</sup> Whereas ssNMR is also applicable for characterizing interprotein interactions,<sup>15; 32; 33</sup> the interpretation of the ssNMR restraints is greatly assisted by knowledge of the docking interface and the oligomeric order, or by additional long-range constraints obtained by other methods.

Such long-range restraints (up to 6 nm for membrane proteins and up to 10 nm in for deuterated soluble proteins<sup>34</sup>) can be obtained from site-directed spin labeling (SDSL) EPR. The method is based on the site-specific labeling of just a few protein side chains with paramagnetic tags, which are based on nitroxides or metal ions (*e.g.*, Cu<sup>2+</sup> or Gd<sup>3+</sup> ions),<sup>35; 36; 37</sup> and observing distance-dependent magnetic (primarily dipolar) interactions between the tags by continuous wave (CW)<sup>38; 39</sup> or time-domain EPR.<sup>34; 40</sup> For example, intermediate-to-short range inter-

monomer contacts in proteorhodopsin (pR) were examined by continuous wave (CW) EPR and the Overhauser dynamic nuclear polarization (DNP) at X-band (9.5 GHz).<sup>41</sup> Long-range electron-electron distances (typically, from 1.6 to 6.0 nm) can be measured by the time-domain double electron-electron resonance (DEER) method.<sup>34; 40</sup> The method has essentially no limitations on the lipids, detergents, or other bilayer mimetics used, and could be used at a high lipid-to-protein ratio. DEER has been recently applied to oligomeric membrane channels<sup>42; 43; 44;</sup><sup>45</sup> and several other important membrane protein complexes.<sup>46; 47; 48; 49; 50</sup> In particular, Thomas, Veglia, and coworkers combined DEER with solution and solid state NMR data to validate the pentameric structure of phospholamban.<sup>50</sup> The groups of Han and Goldfarb derived a structural model for a hexamer formed by pR in frozen micelles from multiple DEER restraints.<sup>49</sup> For the latter study the proteins were labeled with either nitroxides or chelated  $Gd^{3+}$  ions.  $Gd^{3+}$  labeling could be advantageous for DEER, as it leads to smaller artifacts arising from dipolar multispin effects which occur in protein oligomers.<sup>49</sup> The multispin effects on DEER traces have been also explored theoretically for a series of rotationally symmetric polygons<sup>51</sup> and a few well-defined model synthetic polyradical systems. Such studies led to proposing computational strategies for suppressing the DEER “ghost peaks” by data post-processing<sup>52</sup> and by choosing optimal parameters for the pulse EPR sequences.<sup>53</sup>

We note here that DEER restraints are typically measured one at a time for a specific double mutant labeled with paramagnetic tags. Because of a relatively low throughput only a small number of DEER restraints are obtained for a given protein. Furthermore, the accuracy of DEER suffers from some uncertainties in the exact locations of the electronic spins because of the coexistence of multiple rotameric states for the electron spin-bearing side chains.<sup>34; 54</sup>

These existing limitations call for an integration of the NMR and DEER methods in order to expand the number of oligomeric structures that could be solved by magnetic resonance spectroscopy, as well as to improve quality of obtained structures.<sup>55</sup> One example of such an integration was provided by Yang *et al.* for the structure determination of Dsy0195, a water-soluble homodimer (62 amino acids per monomer) from *Desulfitobacterium hafniense*.<sup>56</sup> Specifically, it was shown that an addition of just two DEER restraints to NOE (nuclear Overhauser effect) and PRE (paramagnetic relaxation enhancement) NMR restraints improved the RMSD of the average calculated structure against the crystal structure from 1.51 Å to 1.13 Å.<sup>56</sup>

Here we report on combining long-range DEER distance measurements and ssNMR data for further verification of the oligomeric order and for the structural refinement of a membrane-embedded trimer (~81 kDa) formed by a 7TM photoreceptor *Anabaena* Sensory Rhodopsin (ASR, ~27 kDa) from *Anabaena* sp. PCC7120.<sup>57; 58</sup>

A wealth of biochemical, spectroscopic and ssNMR data show that ASR monomers form stable trimers in cellular *E.coli* membranes,<sup>59</sup> and this state is preserved during the subsequent solubilization in detergents and upon reconstitution in lipids.<sup>29; 60</sup> Furthermore, low-temperature small angle x-ray scattering (SAXS) experiments demonstrated that the ASR trimers are arranged in a hexagonal lattice with the overall geometry similar to that of bR.<sup>59</sup> Yet, the crystallization conditions appear to promote a dissociation of trimers and a subsequent dimerization, as observed in the ASR crystals.<sup>61</sup> Thus, ASR is a notable example of a membrane protein whose oligomeric state depends on the membrane mimetic environment.

Here we present DEER measurements on the oligomeric ASR. We show that by fitting the experimental DEER traces to multispin models, one can discern between possible symmetric



oligomeric states and determine the interspin distances. The results of DEER measurements are consistent with the previously published ssNMR structure. As detailed in the Materials and Method section, preparations of ASR samples, including Cys mutants, labeling with a cysteine-specific nitroxide MTSL, reconstitution in lipid bilayers and the bilayer lipid composition, were essentially the same for both ssNMR PRE and DEER experiments. Both ssNMR and DEER ASR samples also remained fully hydrated. The use of nearly identical experimental protocols – temperature at which DEER and ssNMR measurements are conducted is the only difference – makes the distance restraints obtained by the two methods directly compatible. The DEER restraints were combined with ssNMR structural constraints to refine the high-resolution structure of oligomeric ASR.

## Results and Discussion

For Q-band (34 GHz) DEER and PRE ssNMR measurements two ASR mutants, with the solvent-exposed S26 or N148 residues in the loop regions replaced by Cys, were modified with either a cysteine-specific nitroxide MTSL (S26CR1, N148CR1) or with its diamagnetic analogue MMTS (S26CR1', N148CR1'). Previous ssNMR data showed that these mutations do not cause significant changes in the observed chemical shifts, and, therefore, do not affect the protein fold.<sup>29; 62</sup> Both C26 and C148 are fully accessible and are readily modified by MTSL, as was confirmed by Mass Spectrometry (**Figure S1**). The three other cysteines natively present in ASR at the positions 134, 137, and 203 are not accessible to MTSL labeling as has been shown previously.<sup>29</sup>

While labeling of the solvent exposed loop residues is expected to be less perturbing to the protein structure, a question could be raised regarding temperature-induced changes in the

structure of the flexible loops exposed to water on the membrane surfaces. This could be a concern for DEER measurements conducted at 40 – 77 K whereas ssNMR experiments reported here were performed at 278 K. Firstly, we note that the room temperature continuous wave (CW) X-band (9 GHz) EPR spectra of spin-labeled sidechains S26CR1 and N148CR1 were characteristic of nitroxides approaching intermediate-to-slow motion tumbling regime and, thus, showing a significant immobilization even at room temperature (see Figure S2 for representative examples). Secondly, the DEER samples were flash-frozen in liquid nitrogen before inserting into a precooled EPR cryostat. Such a procedure results in cooling the membrane protein samples to 77 K in less than 1 s whereas the time scale of phase transition in lipid bilayers is typically about 20 s.<sup>63</sup> Finally, the temperature effect on ASR structure is expected to be minimal based on the recent x-ray studies of the homologous BR: the structure obtained by serial millisecond crystallography at room temperature was very similar to the one obtained by conventional x-ray diffraction at 100 K.<sup>64</sup> Thus, we expect the distances measured by DEER at 40 - 77 K and ssNMR at 298 K to be fully comparable.

In this study we limit our consideration of the ASR oligomers to homosymmetric assemblies, *i.e.*, homodimers (such as those observed in the ASR crystals by x-ray<sup>61</sup>), or higher order cyclic oligomers, which are typically found in cells.<sup>65</sup> This assumption is justified by our previous ssNMR observations of all but very few of the ASR residues exhibiting single chemical shift values, which strongly suggests single conformers in the oligomeric ASR assemblies.<sup>66; 67</sup>

**Figure 1** shows representative structures of the symmetric ASR dimers found in crystals (**Figure 1a**, PDB 1XIO<sup>61</sup>), trimers formed upon reconstitution in lipids (**Figure 1b**, PDB 2M3G<sup>60</sup>), and a hypothetical tetrameric structure calculated from the NMR restraints<sup>60</sup> assuming C4 symmetry (**Figure 1c**). The inter-oligomer S26C<sub>β</sub>-S26C<sub>β</sub> and N148C<sub>β</sub>-148C<sub>β</sub> distances for the dimer

(Figure 1a) and electron-electron distances between the indicated spin-labeled chains (Figure 1b and c) are shown as dashed lines.

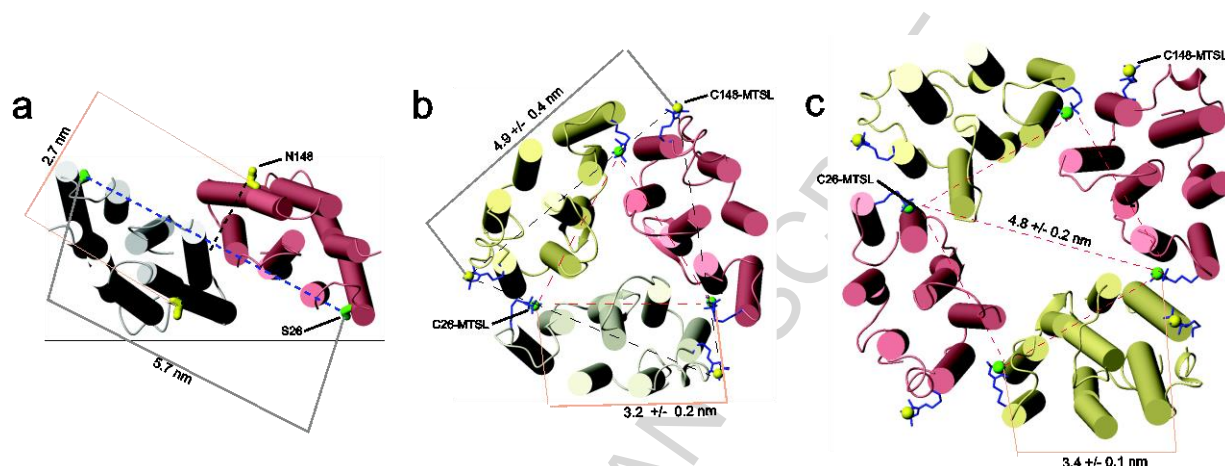


**Fig. 1.** Representative structures of symmetric ASR oligomers constructed from the available X-ray and ssNMR data. (a) X-ray dimer structure (PDB 1XIO)<sup>61</sup> with S26 and N148 highlighted in green and yellow, respectively. C $\beta$ -C $\beta$  (S26-S26) and C $\beta$ -C $\beta$  (N148-N148) distances extracted from the PDB 1XIO are indicated directly in the Figure. (b) ssNMR trimer structure (PDB 2M3G).<sup>60</sup> (c) A hypothetical tetramer calculated from NMR and PRE restraints assuming C4 symmetry. In (b) and (c) the spin-labeled sidechains S26CR1 and N148CR1 are shown in blue with electronic-spin-bearing nitroxide moieties indicated as green and yellow spheres, respectively. Note that the positions of the electron spin-labeled side chains are directly refined from PRE data. The inter-electron distances extracted from the calculated structures in (b) and (c) are indicated in the Figure. See text for further details.

### Effect of diamagnetic dilutions on experimental DEER traces of S26CR1 oligomers

We begin with a discussion of the optimal preparation of ASR samples for DEER measurements. As mentioned in the introduction and further discussed in the sample preparation section, the ASR trimers were found to be initially formed in cellular *E.coli* membranes<sup>59</sup> and persist in detergents.<sup>29</sup> Recent synchrotron SAXS data from purified ASR oligomers reconstituted in DMPC/DMPA lipids under the same conditions as in this work indicate a formation of small 2D crystalline domains of a typical size of 50 nm with a hexagonal lattice parameter of  $\sim 66.4$  Å.<sup>59</sup> Such a close packing of the ASR oligomers could bring multiple nitroxide electronic spins within the DEER distance range and complicate the measurements because of additional contributions from multiple intra- and inter-oligomer electron spin-spin dipolar couplings. Thus, in order to alleviate such complications, ASR samples were

diamagnetically diluted by mixing detergent-solubilized paramagnetically and diamagnetically labeled proteins prior to lipid reconstitution.

We note that a molecular exchange between para- and diamagnetically labeled monomers in the individual ASR oligomers upon this dilution procedure is unlikely because of the high stability of the ASR trimers observed in both lipid bilayers and mild detergents (*e.g.*, DDM). The most direct experimental evidence for the latter has been provided by the largely unchanged inter-monomer PRE effects upon diamagnetic dilution.<sup>29</sup> Thus, a magnetically diluted DEER sample is expected to be composed of a mixture of paramagnetically and diamagnetically labeled oligomers of the same well-defined geometry with no spin dilution occurring within the individual oligomers.

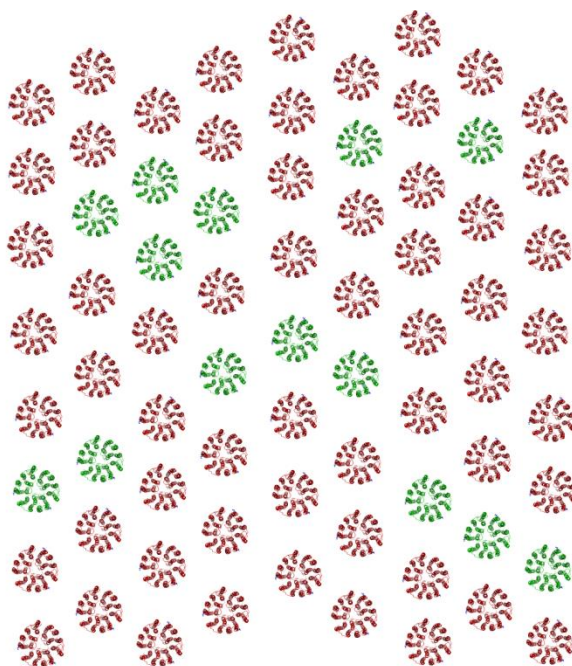


**Fig. 2.** A cartoon representation of a possible distribution of paramagnetic ASR trimers (shown in green) in a lipid-reconstituted 1:4 magnetically diluted sample. Diamagnetically labeled ASR molecules are depicted in red. As further detailed in the text, DDM micelles contain aggregates of 3-4 ASR trimers, and this clustering may persist upon reconstitution, thereby resulting in an incomplete dilution.

Magnetic dilution would not necessarily preclude the proteins from retaining some of the inter-trimer contacts in either detergent or lipid-reconstituted forms. Indeed, a typical molecular weight of the ASR-containing DDM micelles is ~600 kDa.<sup>68</sup> For comparison, the molecular weight of the DDM micelles containing trimers formed by a structurally similar 7TM Halorhodopsin is ~266 kDa,<sup>69</sup> whereas the hexamers of another 7TM protein proteorhodopsin (pR) produce ~340 kDa DDM micelles.<sup>41</sup> Based on this comparison, we thus expect the ASR

DDM micelles to contain clusters of 3 or 4 trimers and such an agglomeration, to persist even upon lipid reconstitution. **Figure 2** illustrates an expected persistence of small clusters of paramagnetic ASR trimers in lipid-reconstituted 1:4 magnetically diluted samples. The space between the ASR trimers is likely to be occupied by bound lipids and other membrane constituents containing sugar moieties as was indicated by the 2D NMR  $^{13}\text{C}$ - $^{13}\text{C}$  correlation spectra.<sup>70</sup> Such remaining clustering as well as possible stacking of ASR in multilamellar lipid-reconstituted samples, could give rise to short intertrimer dipolar contacts between the spin-labeled side chains that may result in an effective shortening of the electronic relaxation time ( $T_2$ ). Furthermore, a possible distribution of local cluster geometries (such as shown in **Figure 2**) would cause an additional decay of the DEER signal without a clear dipolar modulation pattern.

4-Pulse DEER experiment is based on an observation of a dipolar modulation of a refocused primary echo formed by exciting spins A at an observer frequency  $\omega_A$  while the spins B are inverted by  $\pi$ -pulse at a pump frequency  $\omega_B$  applied at time  $t$  after the primary echo (cf. **Figure S3**).<sup>34</sup> While the analysis of ssNMR data relies on observations of fully or partially resolved resonances, the rigid limit EPR spectra of nitroxides attached to different Cys of a protein overlap almost entirely. Furthermore, the excitation bandwidth of the commercial EPR spectrometers is currently insufficient for covering the entire nitroxide spectrum. Therefore, the pump and the observe pulses of the DEER sequence (**Figure S3**) address only a fraction of all the nitroxide spins. For such a spin system the DEER signal  $V(t)$  is given by:<sup>71</sup>

$$V(t) = F(t) \cdot B(t) = (1 - \Delta + F_{Mod}(t)) \cdot B(t), \quad (1)$$

where the form factor  $F(t)$  contains a modulated component  $F_{Mod}(t)$  arising from the dipolar interactions with spins of defined geometry (*i.e.*, between spins in a trimer, etc.),  $\Delta$  is the modulation depth, and  $B(t)$  is a background factor describing dipolar interactions of the observed spins with other spins in the sample (*e.g.*, spins from other oligomers that are within DEER distance range). Parameter  $\Delta$  is determined by a number of spins,  $N$ , having a defined geometry within a cluster as well as experimental parameters, which mainly include the labeling efficiency,  $f$ , and the length,  $t_p$ , and position of the pump pulse with respect to the nitroxide spectrum.

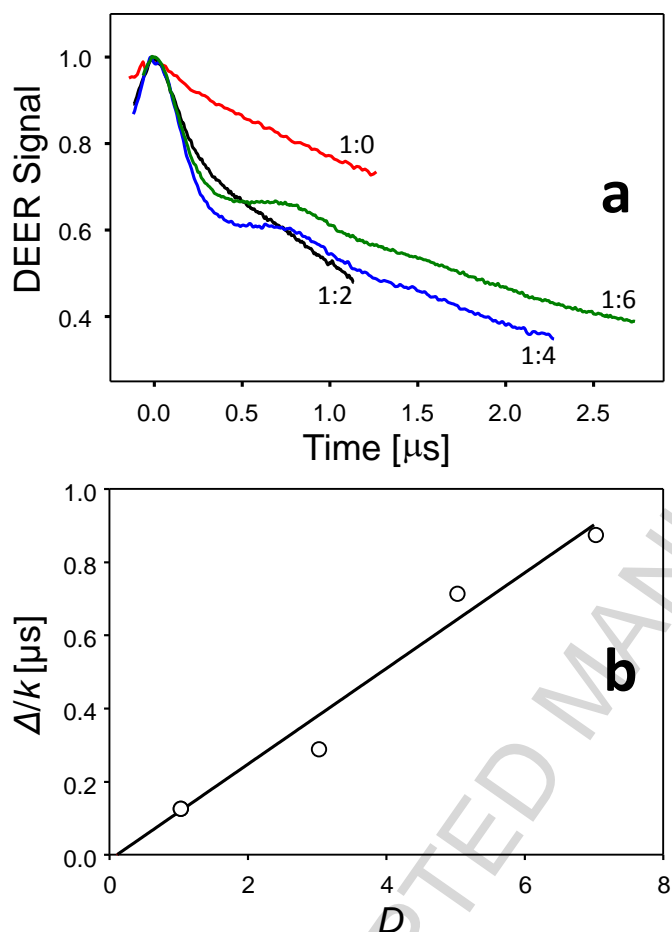


**Fig. 3.** (a) A comparison of experimental DEER traces of ASR samples obtained by mixing paramagnetic S26CR1 and diamagnetic S26CR1' preparations in 1:0 (red line), 1:2 (black line), 1:4 (blue line), and 1:6 (green line) molar ratios. The ratios are also indicated next to the corresponding traces. The modulation depth,  $\Delta$ , and the length of the pump pulse,  $t_p$ , for these experiments are listed in the Table S3. (b) Open circles: DEER modulation depth,  $\Delta$ , normalized by the rate of monoexponential decay,  $k$ , of the unmodulated portion of the signal as a function of the dilution factor,  $D$ , defined as a ratio of all the ASR molecules to those labeled with paramagnetic nitroxides. The solid line is a linear regression with a slope of  $0.134 \pm 0.02 \mu\text{s}$  and an intercept of  $-0.027 \pm 0.008 \mu\text{s}$ .

Initial time-domain Q-band DEER experiments were carried out at an attenuated incident microwave power that yielded relatively long  $\pi$ -pulses at the pump frequency  $\omega_B$  ( $t_p = 28$  to 48 ns, see also **Table S1**). While this choice of  $t_p$  was determined by technical reasons that are outside the scope of this report, we note that a decrease in the excitation bandwidth would decrease the inversion probability,  $\lambda$ , of the pumped B-spins (**Figure S3**) and, therefore, suppress the multispin effects on DEER traces observed for oligomers.<sup>53</sup>

The undiluted S26CR1 sample (the same as used for ssNMR) yielded short electronic relaxation times  $T_{1e}$  and  $T_{2e}$ , and a fast decay of the refocused primary echo that did not allow for collecting the DEER trace longer than 1.3  $\mu$ s (red trace in **Figure 3a**). The DEER trace also lacked dipolar modulation that could be used for reconstruction of the distance distribution. The short electronic relaxation times observed for this sample are indicative of strong inter-electron dipolar interactions. We speculate that such a trace originates from the electronic spins experiencing strong dipolar couplings in a fully paramagnetically labeled ASR lattice.

Dilutions of paramagnetic S26CR1 with diamagnetic S26CR1' resulted in an increase of the electronic relaxation times and slowed down the decay of the modulated portion of the DEER signal (**Figure 3a**). While the DEER trace for the 1:2 diluted sample is still characteristic of strongly coupled electron spins and/or a broad distance distribution, the samples with 1:4 and 1:6 dilution ratios yielded optimal conditions for the DEER signal with a clearly detectable dipolar modulation. We relate this observation to a decrease in the number of potential inter-oligomer electronic spin pairs detectable by DEER. The remaining inter-oligomer dipolar interactions were filtered out by a conventional background correction assuming a monoexponential decay (see Figs. 4 and 5). The monoexponential decay of the DEER signal is typical for a random 3D distribution of the electronic spins. While the ASR trimers reconstituted in lipid bilayers are expected to form fragments of a periodic 2D lattice (*cf.*, **Figure 2**), we do expect a distribution of interoligomer dipolar contacts, which would give rise to a monoexponentially decaying component of the DEER signal.

If a cluster contains  $N$  spins within the DEER distance range, then the DEER modulation depth,  $\Delta$ , for the spins with identical EPR spectra is related to  $N$  as:

$$\Delta = 1 - (1 - \lambda f)^{N-1} \approx (N - 1)\lambda f, \text{ if } \lambda f \ll 1 \quad (2)$$

where  $\lambda$  is the fraction of the spectrum excited by the pump pulse determined by the EPR experimental settings and  $f$  is the labeling efficiency.<sup>34; 46; 72</sup> It was observed that the modulation depth for the experimental DEER traces shown in **Figure 3a** varied over nearly an order of magnitude and generally increased with the magnetic dilution of the ASR samples (**Table S1**). As was discussed above,  $N$  is expected to initially decrease upon magnetic dilution due to a lesser number of the inter-oligomer contacts and then remain  $N \approx \text{const}$  because the individual ASR monomers are non-exchangeable within the trimers, and the small aggregates of the trimers formed in a detergent are expected to persist in lipids upon reconstitution (**Figure 2**). However, such a trend in  $N$  would decrease  $\Delta$  upon dilution, contrary to an increase observed in the experiment (**Figure 3a**).

Further, the observed variations in  $\Delta$  cannot be explained solely by changes in  $\lambda$  due to different lengths of the pump pulse,  $t_p$  (**Table S1**). Indeed, for small values of  $\lambda$ , such as those employed in this work, the excitation bandwidth is  $\sim 1/t_p$  and, therefore, the product  $(\Delta \cdot t_p)$  should not be affected by changes in the parameters of the DEER experiment. We note that for the same bulk protein concentration the labeling efficiency  $f$  is expected to affect the modulation depth  $\Delta$  and the decay rate  $k$  of the unmodulated component of the DEER signal in a similar way: both parameters should be approximately proportional to  $f$ . However, dilution of the labeled ASR oligomers by their diamagnetic analogues is expected to have different effects. Specifically, while the decay rate  $k$  would decrease proportionally to the dilution factor  $D$ , defined as a ratio of the total number of protein molecules in the sample to the number of molecules labeled with paramagnetic nitroxides, the modulation depth  $\Delta$  should remain the same as long as the individual spin-labeled monomers are not exchangeable between the oligomers. Then, since both  $\Delta$  and  $k$  are affected by the length of the pump pulse  $t_p$  in an equal way, the



( $\Delta/k$ ) ratio should increase linearly with the dilution factor,  $D$ . **Figure 3b** shows that the experimental ( $\Delta/k$ ) vs.  $D$  dependence can be well fitted to a straight line with a nearly zero intercept ( $-0.027 \pm 0.008 \mu\text{s}$ ), thus, confirming our hypothesis that the modulated component of the DEER trace stems from the intra-oligomer dipolar interactions, while the background decay is caused by the interactions between different oligomers. Additionally, this serves as a further indication that the number of the interacting nitroxide spins in the ASR oligomers is not reduced upon the diamagnetic dilution, *i.e.*, that the ASR monomers are not exchanged in the magnetically diluted samples. This observation is in the full agreement with the previous conclusions on preserving the intact ASR oligomers in detergents and lipid systems that were obtained by other methods.<sup>29</sup>

### **DEER and PRE NMR rule out formation of ASR dimers in lipid bilayers**

Once the optimal conditions for DEER experiments with ASR reconstituted in lipid bilayers have been established, we turn our attention to the analysis of the background-corrected DEER data. As discussed in the preceding section, magnetic dilution reduces the unwanted electronic spin-spin interactions between different oligomers and simplifies analysis of the DEER signals. Under our sample conditions, we expect the DEER signals to be largely determined by pairwise and multispin effects within the same oligomer, with smaller residual contributions from spin-spin interactions between oligomers. The methodological question we want to address here is whether DEER and ssNMR data can distinguish between different possible oligomeric structures. A comparison of the ASR oligomeric structures and the predicted DEER distances for an X-ray dimer,<sup>61</sup> ssNMR trimer,<sup>60</sup> and a hypothetical tetramer calculated using the previously published NMR data (dihedral restraints derived from the chemical shifts using TALOS+,<sup>73</sup>

inter-nuclear and PRE distance restraints),<sup>60</sup> and assuming C4 symmetry indicates that the spin-spin distances in dimers, trimers, and tetramers are all within the Q-band DEER distance range for membrane protein systems (*i.e.*, < 6 nm, see **Figure 1**). For both the trimer and the tetramer calculations, the distribution of the positions of the paramagnetic C26-MTSL and C148-MTSL sidechains are directly restrained by the PRE measurements (data for S26C ASR mutant were reported earlier;<sup>60</sup> additional PRE measurements on the N148C ASR mutant are discussed below). Following the standard protocols, a total of 100 structures were calculated using ssNMR restraints,<sup>60</sup> each time starting with a randomly generated initial (unfolded) state. Average interspin distances and the standard deviations shown in **Figures 1b** and **c** were estimated from the 10 lowest energy structures.

Although the NMR restraints alone, being of mostly local in nature, cannot distinguish in a reliable manner between the dimer and higher order oligomers, one could employ the long-range DEER constraints to discern the oligomeric order in a straightforward way. For example, let us consider an ASR homodimer of the type observed in the crystalline samples (**Figure 1a**). The standard Tikhonov regularization analysis of the experimental background-corrected DEER trace from a 1:4 dilution S26CR1 sample (**Figure 4a**) using a pairwise spin interaction model and DeerAnalysis2013.2 software<sup>74; 75</sup> yields a narrow distance distribution centered at  $d=3.33$  nm and characterized by a standard deviation  $\sigma=0.21$  nm with no detectable distances outside the 2.8 - 4.0 nm range (**Figure 4a** inset; not shown is the analysis of the DEER trace from the 1:6 S26CR1 dilution sample that yielded essentially identical results). This DEER distance is in an apparent disagreement with the S26-S26 C $\beta$ -C $\beta$  distance of 5.7 nm in the X-ray dimer (**Figure 1a**).

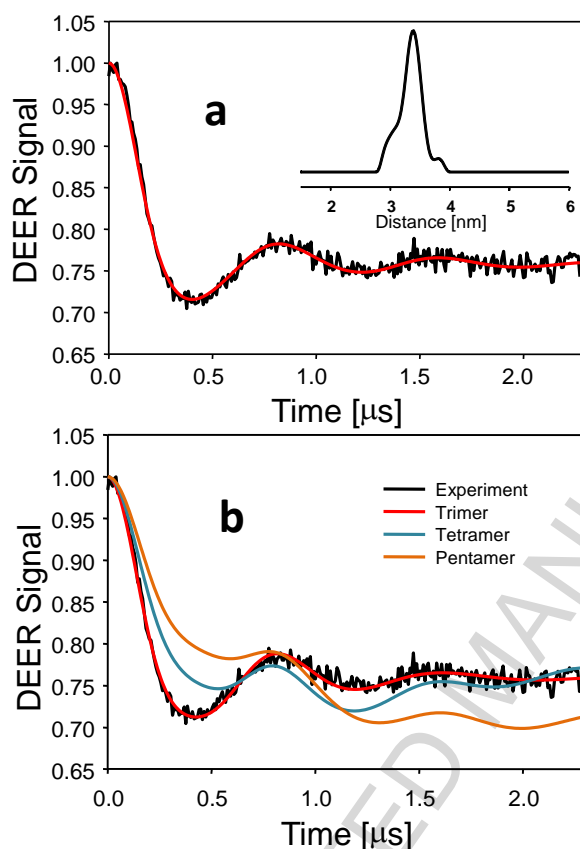


**Fig. 4.** Analysis of an experimental background-corrected Q-band DEER trace measured at  $T=40$  K for spin-labeled S26CR1 ASR oligomers diluted with diamagnetic S26CR1' oligomers in 1:4 molar ratio. **(a)** Results of the Tikhonov regularization analysis (red) assuming only the pairwise spin-spin interactions are superimposed with a baseline-corrected DEER trace shown in black. Inset is the resulting distance distribution with mean  $d=3.33$  nm and the standard deviation  $\sigma=0.21$  nm. **(b)** Simulations of the same DEER trace, but accounting for multispin effects and assuming specific oligomer models: trimer (red), tetramer (blue), and pentamer (green). In each model the interspin distance was assumed to follow a Gaussian distribution with parameters varied during the least-squares optimization. As discussed in the text, the modulation depth was not known *a priori* and was also considered as a fit parameter in the simulations. Only the trimer model yields an acceptable fit with mean  $d=3.38$  nm and  $\sigma=0.16$  nm. See text and the Supplementary Data for further details.

We note that the single DEER restraint obtained for the S26CR1 sample would rule out the formation of the X-ray dimer but not the other possible symmetric dimers and/or higher order oligomers. For these reasons we have carried out additional DEER experiments with the N148CR1 mutant that yielded the second long-range restraint. Similar to S26CR1, the DEER sample was prepared by magnetically diluting N148CR1 with a diamagnetic analogue N148CR1' in a 1:4 molar ratio prior to the lipid reconstitution.

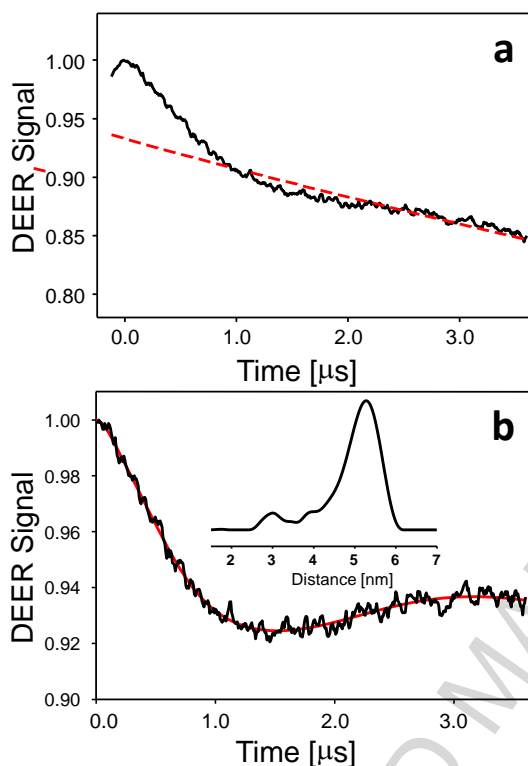


**Fig. 5.** Analysis of N148CR1: N148CR1\* (1:4) DEER data. **(A)** Experimental DEER trace (solid black line) is superimposed with a simulated background decay (dashed red line) **(B)** Baseline-corrected DEER trace (black) is superimposed with simulated DEER traces obtained using the Tikhonov regularization (red) assuming only the pairwise spin-spin interactions. Inset shows the corresponding distance distribution with the dominant feature at mean  $d=5.2$  nm and a standard deviation  $\sigma=0.7$  nm.

The DEER trace revealed a dominant single distance with mean  $d=5.20$  and a standard deviation  $\sigma=0.70$  nm by using the Tikhonov regularization method and assuming pairwise spin interactions (red line in **Figure 5** inset). Calculations of an alternative dimer structure to satisfy the constraints from both mutants using the rigid body docking program, HADDOCK,<sup>76; 77</sup> resulted in only one type of symmetric dimer in a head-to-tail arrangement. To satisfy the DEER S26CR1-S26CR1 restraint of  $3.33\pm0.21$  nm, this arrangement requires the S26CR1 side chains to point towards the hydrophobic core (**Figure S4**). Such an orientation would place the paramagnetic label into the bilayer (for comparison, the DMPC bilayer thickness is  $\sim 4.4\div 4.5$  nm<sup>78</sup>), causing extensive PRE effects in the NMR spectra for the transmembrane residues that

were not observed experimentally.<sup>29</sup> We conclude, therefore, that the conducted DEER measurements with only the two mutants, S26C and N148C, taken together with the PRE NMR data, rule out the dimer formation entirely. Specifically, the dimer observed in ASR crystals (**Figure 1a**) is in apparent disagreement with both DEER and PRE measurements.

### Analysis of higher-order oligomers by DEER

For many systems the relationship between the modulation depth  $\Delta$  of the DEER trace and  $N$  given by eq. (1) provides the means for determination of the oligomeric order if one assumes that each of the monomers could be labeled with an electronic spin and that all  $N$  spins are within the DEER distance range.<sup>34; 42; 46; 72</sup> The application of eq. (1) to ASR oligomers is less straightforward as *a priori* one cannot exclude additional interactions between the ASR oligomers that could bring spin-labeled chains of different oligomers within the DEER distance range and, possibly, result in different electronic relaxation times for different spin clusters. Indeed, as was noted by Borbat and Freed, “the case of several spins can become more complicated if the relaxation times of the spins are significantly different due to different local environments”.<sup>79; 80</sup> Furthermore, while mass spectrometry characterization of the labeled ASR mutants (**Figure S1**) demonstrated a nearly complete labeling, determination of the labeling efficiency by quantitative CW (continuous wave) EPR was not sufficiently accurate primarily because of the problems with measuring ASR concentration due to high optical density of the sample. Finally, we note that PRE NMR data were consistent with the labeling efficiency anywhere from *ca.* 75% to 100%. In addition, one could not also exclude a decrease in labeling efficiency of the DEER samples upon storage because any biogenic reducing agents and/or

catalytic metal ions even in trace amounts are known to chemically reduce the nitroxide to an EPR-silent diamagnetic hydroxylamine.<sup>81; 82; 83; 84; 85</sup>

For these reasons, in order to exclude any ambiguity in determination of the labeling efficiency and to improve the data analysis we turned our attention to direct least-squares fitting analysis of the background-corrected DEER traces. Under our experimental conditions of only a small fraction of the nitroxide spins being excited by the pump pulse, the DEER signal from a multispin system is dominated by dipolar modulations arising from the pairwise spin interactions. However, higher order spin correlations (*e.g.*, 3-spin, 4-spin, and so forth) would still contribute. The latter contributions would give rise to ghost peaks or artifacts in the reconstructed distance distributions when conventional analysis based on the Tikhonov regularization is used.<sup>52</sup> Although such ghost peaks could be suppressed empirically during data processing,<sup>52</sup> or by gradually reducing the experimental parameter  $\lambda$ ,<sup>53</sup> the suppression is incomplete. Thus, we have chosen to fit the experimental DEER traces to the multispin models, assuming that the spins are arranged in the corners of regular polygons. During the simulations, the unknown value of  $(\lambda f)$  was adjusted together with the parameters of the interspin distance distribution(s) given by Gaussian function(s). Examples of such fitting analysis are shown in **Figure 4b** with details of the fitting procedures provided in the Supplementary Data. Specifically, **Figure 4b** shows an excellent agreement between the experiment and the fit to an equidistant trimer model with  $d=3.38\pm0.16$  nm. From the fit the labeling efficiency of the surface cysteine in the S26CR1 trimer was estimated as  $f\approx70\pm10\%$  by taking  $N=3$  and assuming  $\lambda=0.19\pm0.03$  for  $t_p=34$  ns. The high limits of the labeling efficiency can be reconciled with  $f\approx75-100\%$  estimated from PRE NMR.

While for the ASR trimer the DEER trace is defined by the dipolar interactions between the equidistant neighbors, this is not so for the spins in a tetrameric arrangement (**Figure 1c**). For the latter model the contribution from the electron-electron dipolar coupling between the next-nearest (diagonal) neighbors ( $d \approx 4.8$  nm) is expected to affect the DEER trace in a significant way. The blue curve in **Figure 4b** shows the best fit to the tetramer model (explained in **Figure S6**), which explicitly accounts for 2-, 3-, and 4-spin correlations. Although the DEER trace is still dominated by oscillations originating from the pairwise interactions between the two closest neighbors in the tetramer, the contribution from the next nearest “diagonal” neighbors ( $\sim 1/3$  of the total modulation depths), as well as the multispin effects, cause a clear disagreement between the fit and the experiment (**Figure 4b**) even when the modulation depth  $\Delta$  was set as an adjustable parameter. Similarly, the fitting to the equidistant pentamer model (**Figure S7**) fails to reproduce the experimental DEER trace to an even larger degree (**Figure 4b**, green line). Overall, the observed large differences between the simulated DEER traces for trimer, tetramer and pentamer suggest that the least-squares fitting approach can be used for reliable differentiation between the oligomeric states even when the labeling efficiency and/or the inversion factor of the pumped spins are unknown or measured with insufficient accuracy.

In the specific case of ASR, the DEER trace modeling allows us to unambiguously discard all but the trimeric and the dimeric models. We have already discussed that the simultaneous analysis of the DEER data on both S26C and N148C mutants, and PRE data rule out the formation of a symmetric dimer. Whereas both S26CR1-S26CR1 and N148CR1-N148CR1 DEER distance restraints can be simultaneously satisfied in an asymmetric dimeric arrangement, the asymmetry of such a dimer would result in double sets of chemical shifts for

residues at the interface. This is in apparent disagreement with our NMR observations of a highly homogeneous protein as discussed in the beginning of the Results section.

### **Refining the ASR trimer structure by combining ssNMR and long-range DEER restraints**

We now turn our focus to the effects of including the long-range DEER restraints into the calculation of a high-resolution structure of the ASR trimer. Typically, the exact locations of the electronic spins with respect to the protein backbone are somewhat uncertain. One approach to this problem involves molecular dynamics (MD) simulations of the nitroxide sidechains to evaluate the populations of possible rotameric states in order to relate DEER data to  $C_{\alpha}$ - $C_{\alpha}$  distances.<sup>34</sup> Here, we employ an alternative approach of defining conformations of the nitroxide side chains from multiple PRE ssNMR restraints. To better constrain the paramagnetic side chain orientation, we collected additional PRE data on the N148C mutant. The presence of the paramagnetic N148CR1 label is expected to result in a strong attenuation of NMR signals in the vicinity of the label – up to approximately 15 Å in radius.<sup>27</sup> A comparison of 2D ssNMR spectra recorded for the diamagnetically and paramagnetically labeled samples (**Figure 6a**) reveals a limited number of residues whose intensities are significantly attenuated. Consistent with the position of the label at the cytoplasmic side of the helix E, we observe strong PRE effects for the E-F loop (residues G145, I146, T154, T156), which is in a close proximity to the paramagnetic tag. We additionally observe a few more residues with attenuated signals in the cytoplasmic C-D loop and in the cytoplasmic flank of the helix D, *e.g.*, M92 and T100 (**Figure 6**). A small number of restraints observed in the PRE experiment indicate an extended conformation of the modified Cys side chain, likely pointing away from the membrane surface. Nevertheless, the inclusion of the PRE restraints in the structure calculation helps to refine the position of the paramagnetic side chain, as further detailed below.



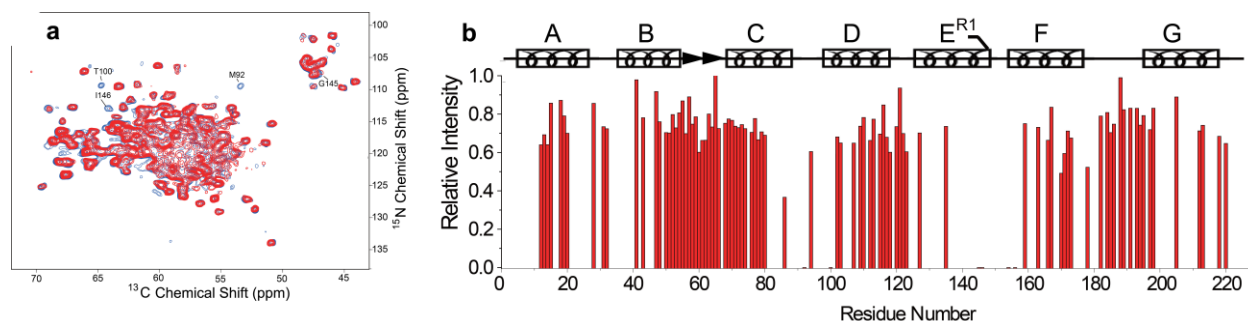


**Fig. 6.** (a) Comparison of 2D NCA spectra between the paramagnetically labeled N148CR1 (red) and its diamagnetic variant N148CR1' (blue). (b) Cross peak intensity ratio  $I_{para}/I_{dia}$  between the N148CR1 and N148CR1' samples. Strong attenuations are seen for the residues M92 and T100, G145, I146, T154, T156, indicating that they are in a close proximity to the electron spin. The secondary structure of ASR and the position of the spin label marked as R1 are shown on top.

Evaluation of the effects of the DEER restraints on the refinement of the ASR oligomer structure has been carried out using two sets of calculations. The first set included all the previously published NMR distances, PRE and the torsional restraints (available from the protein data bank <http://www.rcsb.org> under the PDB ID 2M3G)<sup>60</sup> and the additional PRE restraints obtained for the N148CR1 sample (a total of 2,838 restraints per monomer). The second set included all of the above and the additional DEER S26CR1-S26CR1 and N148CR1-N148CR1 restraints (a total of 2,838 restraints per monomer with two additional DEER restraints for the trimer, see **Table S2** for summary). Both calculations were performed using the program CNS (version 1.21).<sup>86</sup>

In order to include the DEER distance restraints in the structural calculations of the trimeric ASR, the cysteine side chains of both C26 and C148 were replaced with nitroxide side chains (R1). As determined from DEER experiments, the electron-electron distance between the NO moieties of C26R1 of the neighboring monomers was  $33.8 \pm 1.6 \text{ \AA}$ , while the distance between the NO moieties of C148R1 was  $52.0 \pm 7.0 \text{ \AA}$ . Those distances were included in the structure calculation by converting to the distance restraints between the NO atoms of C26R1 from the neighboring monomers with an upper bound of  $35.4 \text{ \AA}$  and with a lower bound of  $32.2$

Å, and between the NO atoms of C148R1 of the neighboring monomers with an upper bound of 59.0 Å and with a lower bound of 45.0 Å. The calculation procedure involved the generation of 100 random structures sampled at 10,000 K and followed by a simulated annealing to 50 K. Both DEER and NMR restraints were considered during the annealing stages (including the PRE restraints). The force field parameters and topology of R1 were adopted from those reported by Sammalkorpi and Lazaridis.<sup>87</sup> No additional restraints were set to fix the R1 sidechains, allowing for sampling of all the possible conformations. In such a manner, the R1 sidechain conformations and orientations were determined by the local constraints from the PRE experiments and the long-range constraints from DEER measurements.

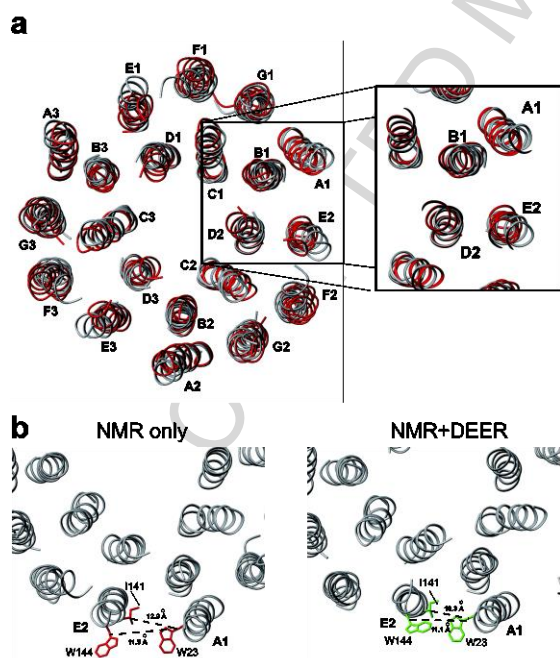


**Fig. 7.** Refinement of the ASR trimer structure by including DEER restraints in the structure calculations. **(a)** Comparison of the two trimeric structures calculated using the NMR only (grey) and the NMR and DEER restraints (red) viewed from the cytoplasmic side. The interfacial region (helices A1, B1, D2, E2) of the two interacting monomers are shown on the right. Loops are omitted for clarity. **(b)** Interhelical packing between helices A1 and E2 at the interface. Selected side chains on the cytoplasmic side are indicated with  $C_{\beta}$ - $C_{\beta}$  distances shown as dashed lines. Note that this region lacks the internuclear distance restraints and orientations of the side chains are poorly defined.

An ensemble of 10 lowest-energy structures from a set of 100 structures constructed using DEER+NMR data had RMSD of 0.6 Å for the backbone atoms of the secondary structures. A reference ensemble of ASR structures was also obtained using the NMR restraints only and the lowest energy structure is superimposed with the DEER+NMR structure for a comparison (**Figure 7**). Root mean square deviations between the helical regions of the lowest energy structures determined using DEER and NMR restraints, and the NMR restraints alone are 1.4 and 2.7 Å for the backbone and the heavy side chains atoms, respectively. Overall, the refinement has the most pronounced effect on the cytoplasmic side as further detailed below.

Specifically, analysis of these two structures revealed that the addition of the DEER data results in ~3 Å shift of the cytoplasmic end of the helix D towards the core of the proteins, as measured using the C<sub>α</sub> atoms of L100 of the two structures (**Figure 7a**). This value is larger than the sum of the local RMSD of the C<sub>α</sub> of L100 in the NMR-only structure ensemble, 1.2 Å, and in the NMR+DEER structure ensemble, 1.0 Å.

The NMR+DEER structures show tighter inter-monomer packing than the ones obtained from NMR data alone (**Figure 7b**). For example, the distances from helix A of one monomer to helix E of the neighboring monomer are *ca.* 2-3 Å shorter, as measured between C<sub>β</sub> atoms of W23 of helix A and I141 of helix E and between W23 of helix A and W143 of helix E. The extent of the reported structure refinement should be considered in the context of the conformational changes occurring during the ASR functional cycle. Although there is no high-resolution experimental data available on the structural rearrangements occurring during the ASR photo-cycle, a relevant scale may be estimated from homologous proteins such as SRII: as derived from EPR measurements, the relative displacements are on the order of 2-4 Å for helices G and F, respectively.<sup>88; 89; 90</sup> Thus, a 2-3 Å displacement of helices in the refined structure of

ASR could be indeed important for correctly resolving conformational changes in the protein photo-cycle. The refined structure has been deposited in the protein data bank [www.rcsb.org](http://www.rcsb.org) under the accession code 5UK6.

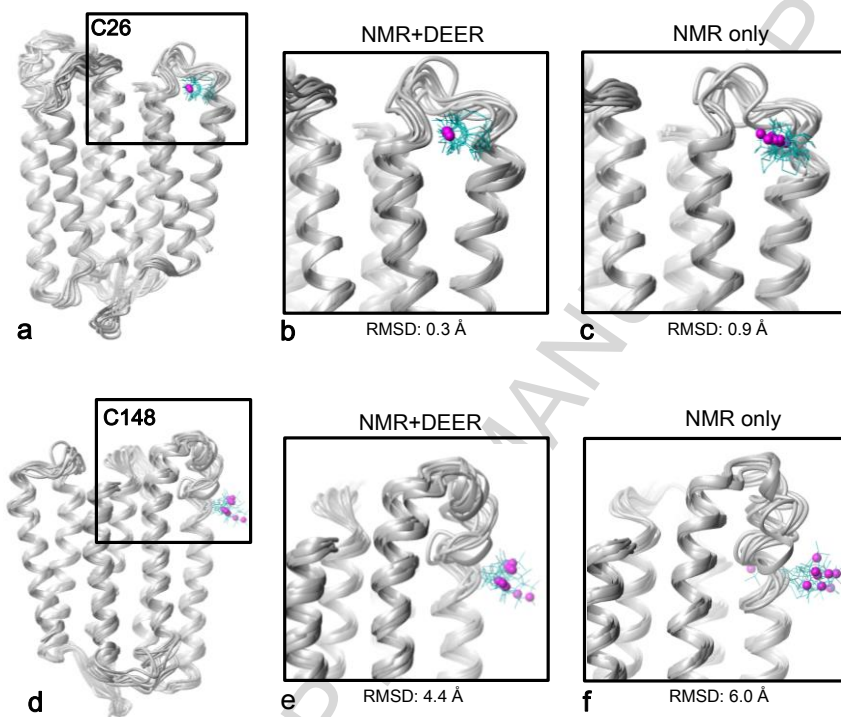


**Fig. 8.** Refinement of the local structure of spin-labeled ASR sidechains by combining DEER and NMR data. **(a and d)** Ensembles of 10 lowest energy structures (out of 100) of the monomer ASR from trimers determined by combining NMR and DEER restraints. The squares enclose the magnified regions. **(b-c)** Enlargements compare a convergence of the ensembles of the local region around the paramagnetic C26R1 obtained from the combined NMR and DEER restraints **(b)** and from the NMR restraints only **(c)**. **(d-e)** The enlargements compare a convergence of the ensembles of the local region around the paramagnetic C148R1 obtained from the combined NMR and DEER restraints **(e)** and from the NMR restraints only **(f)**. The nitroxide R1 sidechains are shown as green sticks and the NO moieties are shown as magenta balls. The RMSD values calculated for NO moieties are listed below the corresponding enlargements.

Finally, an addition of the DEER restraints reduced the local disorder of C26 and C148 side chains. RMSD of NO moieties were calculated from the ensemble of structures obtained from combining NMR and DEER restraints and the NMR-restraints only (**Figure 8**). The NMR-DEER ensemble displays lower RMSDs for the spin-labeled sidechains. Specifically, the RMSD of C26R1 decreased from 0.9 to 0.3 Å. For C148R1, the RMSD changes were from 3.8 to 3.1 Å (**Figure 8**). The RMSD values provide a clear indication that the nitroxide chain of C26R1 is

significantly restrained with respect to the protein whereas C148R1 exists in multiple rotameric conformations. This data is in a qualitative agreement with DEER results that showed a narrow distance distribution for the C26R1 spin pairs and a broader spread of distances for C148R1 (*cf.* **Figs. 4a** and **5b**).

## SUMMARY

In summary, we have shown that the homotrimer structure of a heptahelical microbial photoreceptor ASR in native lipid bilayers could be further refined by adding just two additional long-range DEER distance restraints to a large number of short (*i.e.*, internuclear distances and torsional angles) and intermediate intra- and intermonomer PRE restraints available from ssNMR data. The inclusion of the DEER restraints in the ssNMR structure calculation protocol has a noticeable effect on the positions of the transmembrane helices, primarily resulting in an overall more compact fold of the trimer and in better defined positions of the side chains at the interface. The magnitude of the reported structure refinement, including the relative displacements of *ca.* 2-3 Å for helices A1 and E2, is comparable to typical conformational changes occurring in the photocycle of retinal proteins: helical displacements in the homologous sensory rhodopsin SRII are *ca.* 2-4 Å.<sup>88</sup> Positions of the side chains bearing paramagnetic nitroxide tags become better defined and the use of the available ssNMR PRE data eliminates the need for additional MD simulations to relate the positions of the electronic spins with respect to the protein backbone – a procedure that is typically employed in DEER-only studies of protein assemblies and protein conformational changes.<sup>34</sup>

Our approach can be applied to other oligomeric membrane proteins, provided that the paramagnetic labels, nitroxide radicals and/or other paramagnetic tags, can be introduced into the

protein background. In the case of ASR presented here, two DEER distance constraints could be extracted without prior knowledge of the oligomeric structure, and were in excellent agreement with the data previously determined by a combination of NMR, and other biophysical and biochemical methods.<sup>29; 60</sup>

Importantly, DEER measurements can be carried out on membrane proteins reconstituted in the physiologically relevant environment of lipid bilayers using essentially the same preparations protocols as used for solid-state NMR measurements. The combined set of NMR and DEER structural constraints for membrane proteins typically spans the range of 3-60 Å and even longer for deuterated samples, and is suitable for the simultaneous characterization of both the atomic level structure, and oligomeric and potentially long-range oligomer organizations.

## MATERIALS AND METHODS

### A. Materials and protein samples

**Materials.** Common chemicals of a reagent grade were purchased from either Fisher Scientific (Unionville, ON, Canada) or Sigma-Aldrich (Oakville, ON, Canada). <sup>15</sup>N-labeled ammonium chloride and <sup>13</sup>C<sub>6</sub>-glucose were purchased from Cambridge Isotope Laboratories (Andover, MA, USA). Lipids were purchased from Avanti Polar Lipids (Alabaster, AL).

**Expression and purification of ASR.** S26C and N148C mutants of ASR were produced as described earlier.<sup>29; 62</sup> Both mutants were expressed in BL21-Codonplus-RIL *E. coli* cells following a previously described protocol.<sup>66</sup> Uniformly <sup>15</sup>N- and <sup>13</sup>C-labeled ASR was produced from cells grown in a minimal medium containing 1 g of <sup>15</sup>NH<sub>4</sub>Cl and 4 g of <sup>13</sup>C-glucose per liter of culture as the sole nitrogen and carbon sources. Retinal was added exogenously at a

concentration of 7.5  $\mu\text{M}$  to regenerate the expressed opsin. Cells were broken by sonication and the membrane fraction was solubilized in 1 % DDM (*n*-dodecyl  $\beta$ -D-maltoside). The protein was purified following the batch protocol as described in the Qiagen  $\text{Ni}^{2+}$ -NTA manual (Qiagen, Mississauga, ON, Canada). The final yields of the S26C and N148C mutants were approximately 3.5 mg and 6.5 mg per liter of culture, respectively. Protein concentration was determined by measuring the absorbance of the opsin-bound retinal using an extinction coefficient of  $48,000 \text{ M}^{-1}\text{cm}^{-1}$ .<sup>91</sup>

**Paramagnetic spin labeling.** For PRE and DEER experiments, purified S26C (or N148C) ASR were buffer-exchanged using Amicon Ultra-15 10K centrifugal filters (Millipore, Massachusetts, MA, USA) into pH 8.0 buffer (5 mM Tris, 10 mM NaCl, 0.05% DDM), and concentrated to  $\sim 1 \text{ mg/ml}$  (36  $\mu\text{M}$ ). The protein was incubated for 1 h at room temperature (22 °C) with a twenty-fold molar excess of a nitroxide spin labeling reagent MTSL (S-(1-oxyl-2,2,5,5-tetramethyl-2,5-dihydro-1H-pyrrol-3-yl)methyl methanesulfonothioate, Toronto Research Chemicals Inc., ON, Canada).<sup>92</sup> The unreacted MTSL was removed by dialysis. The cysteine spin labeling was monitored by MALDI TOF and HPLC-ESI-Q-TOF Mass Spectrometry. The molecular weight of the spin labeled S26C or N148C mutants (called S26CR1 or N148CR1 in the following) was found to be  $\sim 184$  and 194 Da higher than those of the unmodified proteins (**Figure S2**, Supplementary Data).

**Preparation of diamagnetically labeled proteins.** The S26C and N148C mutants were reacted with methyl methanethiosulfonate (MMTS, purchased from Toronto Research Chemicals Inc., ON, Canada)<sup>93; 94</sup> using the protocol described above for the MTSL labeling.

**Sample preparation for ssNMR and DEER.** PRE measurements on S26C were reported previously.<sup>29</sup> Additional PRE experiments were conducted with  $^{13}\text{C}$ -,  $^{15}\text{N}$ -, and paramagnetically-labeled N148CR1 that was diluted with diamagnetically labeled natural abundance N148CR1' (molar ratio of 1:2). Isotopically  $^{13}\text{C}$ -,  $^{15}\text{N}$ -labeled diamagnetic N148CR1' diluted with the natural abundance N148CR1' (molar ratio of 1:2) was used as a reference. For the dilution, isotopically labeled and detergent-solubilized N148CR1 (or N148CR1') was mixed with the solubilized natural abundance N148CR1' and stirred for 1 h at room temperature prior to the reconstitution. This dilution ratio with the NMR-silent protein was chosen in order to pack the paramagnetically labeled and the diamagnetic reference NMR samples with approximately equal amount of N148CR1 and N148CR1' proteins to allow for a proper comparison of the cross peak intensities.

All the proteins were dissolved in a pH 8.0 buffer (5 mM Tris, 10 mM NaCl, 0.05% DDM) and reconstituted with DMPC/DMPA (Avanti Polar Lipids, Alabaster, AL, USA) liposomes at a protein:lipid ratio of 2:1 (w/w). Liposomes were prepared by hydrating DMPC:DMPA lipids mixed at a 9:1 ratio (w/w) with a pH 8.0 buffer (5 mM Tris, 10 mM NaCl). Protein and lipid concentrations were 2.3 and 1.15 mg/mL, respectively. DDM detergent was removed by Bio-beads (SM-II, Bio-Rad Laboratories, Inc., Hercules, CA, USA). The final protein:lipid ratio in the proteoliposomes was confirmed using transmission FTIR spectroscopy (IFS 66v/S Vacuum FTIR, Bruker Optics, Germany) by comparing the vibration intensities of the lipid esters (at  $\sim 1740\text{ cm}^{-1}$ ) and the protein backbone carbonyls (amide I).<sup>95</sup> For NMR measurements, proteoliposomes were collected by ultracentrifugation at  $150,000\times g$  for 1 h. Approximately 10.5 mg of the total protein was center-packed in a thin-wall 3.2 mm rotor; the amount of isotopically  $^{13}\text{C}$ -,  $^{15}\text{N}$ -labeled ASR was  $\sim 3.5$  mg. Previously, a comparison of water



and the lipid  $^1\text{H}$  peak intensities and determination of 18:1 lipid-to-protein ratio from FTIR measurements yielded an estimate of about 4,000 water molecules per monomeric ASR under the same sample preparation procedures.<sup>62</sup> Thus, the ASR samples for ssNMR are fully hydrated.

Similar protocols were used to prepare samples for DEER measurements except for the following modifications: (i) S26CR1 was prepared as undiluted and diluted with the diamagnetic S26CR1' analogue at the 1:2, 1:4, and 1:6 molar ratios. (ii) Only magnetically diluted N148CR1 with N148CR1' in a 1:4 molar ratio was used. (iii) Upon the detergent removal and lipid reconstitution, the aqueous dispersions of the proteoliposomes were spun down for 3 min at ca. 3,000 $\times g$  and the bottom fraction was drawn into a Suprasil WG-222T (o.d.=1.6 mm, i.d.=1.1 mm) tubes (Wilmad LabGlass, Vineland, NJ, USA) sealed from one end. The proteoliposomes in the Suprasil tube were spun again for 3 min at 3,000 rpm to pack the sample at the bottom of the tube. The clear supernatant was removed from the top portion of the tube, additional proteoliposomes were added, and the procedure was repeated till the bottom 1.0-1.5 cm of the tube was packed with the proteoliposomes. Such a procedure resulted in ASR samples retaining significant amount of bulk water and ensured full protein hydration. The bulk water does not directly interact with the protein and is expected to have a minimal, if any, effect on the ASR structure. No cryoprotectant was used for DEER measurements.

## B. Experimental Methods

**MAS ssNMR spectroscopy.** MAS ssNMR spectra were acquired on a Bruker Avance III spectrometer operating at 800.230 MHz, equipped with a 3.2 mm Efree  $^1\text{H}/^{13}\text{C}/^{15}\text{N}$  probe (Bruker Biospin, Billerica, MA, USA). The experiments were conducted at a spinning frequency

of 14.3 kHz and at an effective sample temperature of 5 °C. Typical  $\pi/2$  pulses were 2.5  $\mu$ s for  $^1\text{H}$ , 4  $\mu$ s for  $^{13}\text{C}$ , and 6  $\mu$ s for  $^{15}\text{N}$ , respectively. SPINAL64 decoupling of ~84 kHz was used during indirect and direct chemical shift evolutions.<sup>96</sup>

For 2D NCA correlation spectra  $^1\text{H}/^{15}\text{N}$  cross-polarization (CP) contact time was 300  $\mu$ s, with a constant radio-frequency (r.f.) field of ~40 kHz on nitrogen, and proton r.f. intensity ramped linearly around the  $n=1$  Hartmann-Hahn condition.<sup>97</sup>  $^{15}\text{N}/^{13}\text{C}\alpha$  band-selective cross polarization<sup>98</sup> was implemented with a contact time of 5 ms. Nitrogen r.f. intensity was adjusted to ~35.7 kHz, and carbon r.f. field was ramped linearly around ~21.4 kHz. The CW decoupling during the  $^{15}\text{N}/^{13}\text{C}$  CP steps was 90 kHz. The time domain matrix of NCA experiments was 160 ( $t_1$ )  $\times$  2048 ( $t_2$ ), with  $t_1$  and  $t_2$  increments of 148  $\mu$ s and 10  $\mu$ s, respectively. 304 scans were recorded with a recycle delay of 1.7 s, which resulted in a total acquisition time of 24 h.

Data sets were processed using NMRpipe,<sup>99</sup> and the chemical shifts were indirectly referenced to 2,2-dimethyl-2-silapentane-5-sulfonic acid (DSS).<sup>100</sup> The peak intensities of the well-resolved non-overlapping cross peaks in the NCA spectra were analyzed using SPARKY<sup>101</sup> to derive the paramagnetic relaxation enhancements.

**EPR and DEER Spectroscopy.** Preliminary continuous wave (CW) EPR experiments were carried out at X-band (9 GHz) using a Varian Century Series EPR spectrometer (Palo Alto, CA).

DEER spectra were measured at Q-band (34 GHz) using the dead-time-free four pulse sequence (**Figure S3**),<sup>102</sup> and a custom-built Bruker ELEXSYS E580 spectrometer equipped with SuperQ-FT bridge and SuperQ-FT Solid State 10 W Amplifier (all from Bruker Biospin, Billerica, MA, USA). The temperature was stabilized using a Bruker ER 4118CF flow cryostat operated with either liquid nitrogen or helium. For preliminary measurements the temperature

was set to 77 K while the final measurements were carried out at 40 K to take advantage of longer electronic relaxation times for collecting the DEER traces. In a typical DEER experiment (**Figure S3**) the pump and the observer frequencies were set as  $\nu_2=34.008$  GHz and  $\nu_1=33.964$  GHz, respectively, and magnetic field was fixed at 12,103.5 G to obtain the maximum of the echo-detected signal at the pump frequency (*i.e.*, to maximize the fraction of the pumped B spins). Positions of the three observer pulses were fixed with the separation between the first and the second pulse of  $\tau_1=200$  ns and the separation between the second and the third pulse of  $\tau_2=2,600$  ns. The lengths of the observer pulses were 36 and 72 ns for the  $\pi/2$ - and  $\pi$ -pulses respectively. The pump pulse of either 34 or 48 ns length was stepped in 4 ns increments over the range of 2,400 ns.

#### Accession numbers

PDB ID: 5UK6

#### Acknowledgments

This research was supported by U.S. DOE Contract DE-FG02-02ER15354 to AIS (DEER experiments and DEER trace modelling) and NSERC Discovery Grants RGPIN-2014-04547 to VL and RGPIN-2013-250202 to LSB. SW acknowledges the support of the Natural Science Foundation of China (31470727), the National Key Research and Development Program from the Ministry of Science and Technology of the People's Republic of China (contract number 2016YFA0501203), the Beijing National Laboratory for Molecular Sciences, and the Recruitment Program of Global Youth Experts. SM acknowledges support of NSF (DBI-1229547). TIS acknowledges support of NSF (CHE-0840501). EPR instrumentation was supported by grants from the National Institutes of Health (no. RR023614), the National Science

Foundation (no. CHE-0840501), and NCBC (no. 2009-IDG-1015). RAM and MEW were recipients of the Ontario Graduate Scholarship. We thank Drs. A. Charchoglyan and D. Brewer of the University of Guelph Advanced Analysis Centre for help with MassSpec data collection and analysis and Prof. M. A. Voinov (NCSU) for insightful discussions.

### **Supplementary Data**

Supplementary data associated with this article including mass spectrometry data, continuous wave X-band EPR spectra, DEER pulse sequence, DEER fitting procedures, and details of structure calculation can be found, in the online version, at doi:(to be filled by the Editorial Office).

## References

1. Popot, J. L. & Engelman, D. M. (1990). Membrane protein folding and oligomerization: the two-stage model. *Biochemistry* **29**, 4031-4037.
2. Furthmayr, H. & Marchesi, V. T. (1976). Subunit Structure of Human Erythrocyte Glycophorin-A. *Biochemistry* **15**, 1137-1144.
3. Holsinger, L. J. & Lamb, R. A. (1991). Influenza virus M2 integral membrane protein is a homotetramer stabilized by formation of disulfide bonds. *Virology* **183**, 32-43.
4. Clarke, O. & Gulbis, J. (2012). Oligomerization at the Membrane. In *Protein Dimerization and Oligomerization in Biology* (Matthews, J., ed.), Vol. 747, pp. 122-136. Springer New York.
5. Ferre, S. & Franco, R. (2010). Oligomerization of G-protein-coupled receptors: a reality. *Curr Opin Pharmacol* **10**, 1-5.
6. Cortes, D. M. & Perozo, E. (1997). Structural Dynamics of the Streptomyces lividans K<sup>+</sup> Channel (SKC1): Oligomeric Stoichiometry and Stability. *Biochemistry* **36**, 10343-10352.
7. Valiyaveetil, F. I., Zhou, Y. & MacKinnon, R. (2002). Lipids in the structure, folding, and function of the KcsA K<sup>+</sup> channel. *Biochemistry* **41**, 10771-7.
8. Fleming, K. G., Ackerman, A. L. & Engelman, D. M. (1997). The effect of point mutations on the free energy of transmembrane alpha-helix dimerization. *J Mol Biol* **272**, 266-75.
9. Gell, D. A., Grant, R. P. & Mackay, J. P. (2012). The detection and quantitation of protein oligomerization. *Adv Exp Med Biol* **747**, 19-41.

10. Adair, B. D. & Engelman, D. M. (1994). Glycophorin A helical transmembrane domains dimerize in phospholipid bilayers: a resonance energy transfer study. *Biochemistry* **33**, 5539-44.
11. Columbus, L., Lipfert, J., Jambunathan, K., Fox, D. A., Sim, A. Y. L., Doniach, S. & Lesley, S. A. (2009). Mixing and Matching Detergents for Membrane Protein NMR Structure Determination. *Journal of the American Chemical Society* **131**, 7320-7326.
12. Zhou, H. X. & Cross, T. A. (2013). Influences of membrane mimetic environments on membrane protein structures. *Annual review of biophysics* **42**, 361-92.
13. Heyn, M. P., Cherry, R. J. & Dencher, N. A. (1981). Lipid--protein interactions in bacteriorhodopsin--dimyristoylphosphatidylcholine vesicles. *Biochemistry* **20**, 840-9.
14. Klyszejko, A. L., Shastri, S., Mari, S. A., Grubmuller, H., Muller, D. J. & Glaubitz, C. (2008). Folding and assembly of proteorhodopsin. *J Mol Biol* **376**, 35-41.
15. Maciejko, J., Mehler, M., Kaur, J., Lieblein, T., Morgner, N., Ouari, O., Tordo, P., Becker-Baldus, J. & Glaubitz, C. (2015). Visualizing Specific Cross-Protomer Interactions in the Homo-Oligomeric Membrane Protein Proteorhodopsin by Dynamic-Nuclear-Polarization-Enhanced Solid-State NMR. *Journal of the American Chemical Society* **137**, 9032-9043.
16. Hussain, S., Kinnebrew, M., Schonenbach, N. S., Aye, E. & Han, S. (2015). Functional Consequences of the Oligomeric Assembly of Proteorhodopsin. *Journal of Molecular Biology* **427**, 1278-1290.
17. Zeev-Ben-Mordehai, T., Vasishtan, D., Siebert, C. A. & Grünewald, K. (2014). The full-length cell-cell fusogen EFF-1 is monomeric and upright on the membrane. *Nat Commun* **5**, 3912.

18. Lau, W. C. Y. & Rubinstein, J. L. (2012). Subnanometre-resolution structure of the intact *Thermus thermophilus* H<sup>+</sup>-driven ATP synthase. *Nature* **481**, 214-218.
19. Yeow, E. K. L. & Clayton, A. H. A. (2007). Enumeration of Oligomerization States of Membrane Proteins in Living Cells by Homo-FRET Spectroscopy and Microscopy: Theory and Application. *Biophysical Journal* **92**, 3098-3104.
20. McDermott, A. (2009). Solid state NMR studies of enzymes and membrane proteins. *Annual review of biophysics* **38**, 385-403.
21. Tang, M., Comellas, G. & Rienstra, C. M. (2013). Advanced solid-state NMR approaches for structure determination of membrane proteins and amyloid fibrils. *Acc Chem Res* **46**, 2080-8.
22. Baker, L. A. & Baldus, M. (2014). Characterization of membrane protein function by solid-state NMR spectroscopy. *Curr Opin Struct Biol* **27**, 48-55.
23. Wang, S. & Ladizhansky, V. (2014). Recent advances in magic angle spinning solid state NMR of membrane proteins. *Prog Nucl Magn Reson Spectrosc* **82**, 1-26.
24. Murray, D. T., Das, N. & Cross, T. A. (2013). Solid state NMR strategy for characterizing native membrane protein structures. *Acc Chem Res* **46**, 2172-81.
25. Radoicic, J., Lu, G. J. & Opella, S. J. (2014). NMR structures of membrane proteins in phospholipid bilayers. *Q Rev Biophys* **47**, 249-83.
26. Balayssac, S., Bertini, I., Bhaumik, A., Lelli, M. & Luchinat, C. (2008). Paramagnetic shifts in solid-state NMR of proteins to elicit structural information. *Proc Natl Acad Sci U S A* **105**, 17284-9.

27. Nadaud, P. S., Helmus, J. J., Hofer, N. & Jaroniec, C. P. (2007). Long-range structural restraints in spin-labeled proteins probed by solid-state nuclear magnetic resonance spectroscopy. *J Am Chem Soc* **129**, 7502-3.
28. Nadaud, P. S., Helmus, J. J., Kall, S. L. & Jaroniec, C. P. (2009). Paramagnetic ions enable tuning of nuclear relaxation rates and provide long-range structural restraints in solid-state NMR of proteins. *J Am Chem Soc* **131**, 8108-20.
29. Wang, S. L., Munro, R. A., Kim, S. Y., Jung, K. H., Brown, L. S. & Ladizhansky, V. (2012). Paramagnetic Relaxation Enhancement Reveals Oligomerization Interface of a Membrane Protein. *Journal of the American Chemical Society* **134**, 16995-16998.
30. Li, J., Pilla, K. B., Li, Q., Zhang, Z., Su, X., Huber, T. & Yang, J. (2013). Magic Angle Spinning NMR Structure Determination of Proteins from Pseudocontact Shifts. *Journal of the American Chemical Society* **135**, 8294-8303.
31. Jaroniec, C. P. (2015). Structural studies of proteins by paramagnetic solid-state NMR spectroscopy. *Journal of Magnetic Resonance* **253**, 50-59.
32. Antzutkin, O. N., Balbach, J. J., Leapman, R. D., Rizzo, N. W., Reed, J. & Tycko, R. (2000). Multiple quantum solid-state NMR indicates a parallel, not antiparallel, organization of beta-sheets in Alzheimer's beta-amyloid fibrils. *Proceedings of the National Academy of Sciences of the United States of America* **97**, 13045-13050.
33. Can, T. V., Sharma, M., Hung, I., Gor'kov, P. L., Brey, W. W. & Cross, T. A. (2012). Magic angle spinning and oriented sample solid-state NMR structural restraints combine for influenza A M2 protein functional insights. *J Am Chem Soc* **134**, 9022-5.
34. Jeschke, G. (2012). DEER distance measurements on proteins. *Annual Review of Physical Chemistry* **63**, 419-46.



35. Cunningham, T. F., Shannon, M. D., Putterman, M. R., Arachchige, R. J., Sengupta, I., Gao, M., Jaroniec, C. P. & Saxena, S. (2015). Cysteine-Specific Cu<sup>2+</sup> Chelating Tags Used as Paramagnetic Probes in Double Electron Electron Resonance. *The Journal of Physical Chemistry B* **119**, 2839-2843.
36. Cunningham, T. F., Putterman, M. R., Desai, A., Horne, W. S. & Saxena, S. (2015). The Double-Histidine Cu<sup>2+</sup>-Binding Motif: A Highly Rigid, Site-Specific Spin Probe for Electron Spin Resonance Distance Measurements. *Angewandte Chemie* **54**, 6330–6334.
37. Gordon-Grossman, M., Kaminker, I., Gofman, Y., Shai, Y. & Goldfarb, D. (2011). W-Band pulse EPR distance measurements in peptides using Gd<sup>3+</sup>-dipicolinic acid derivatives as spin labels. *Physical Chemistry Chemical Physics* **13**, 10771-10780.
38. Rabenstein, M. D. & Shin, Y. K. (1995). Determination of the Distance between Two Spin Labels Attached to a Macromolecule. *Proc Natl Acad Sci U S A* **92**, 8239-8243.
39. Hustedt, E. J., Smirnov, A. I., Laub, C. F., Cobb, C. E. & Beth, A. H. (1997). Molecular distances from dipolar coupled spin-labels: The global analysis of multifrequency continuous wave electron paramagnetic resonance data. *Biophysical Journal* **72**, 1861-1877.
40. Borbat, P. P., Costa-Filho, A. J., Earle, K. A., Moscicki, J. K. & Freed, J. H. (2001). Electron spin resonance in studies of membranes and proteins. *Science* **291**, 266-269.
41. Stone, K. M., Voska, J., Kinnebrew, M., Pavlova, A., Junk, M. J. & Han, S. (2013). Structural insight into proteorhodopsin oligomers. *Biophysical Journal* **104**, 472-81.
42. Endeward, B., Butterwick, J. A., MacKinnon, R. & Prisner, T. F. (2009). Pulsed Electron-Electron Double-Resonance Determination of Spin-Label Distances and

- Orientations on the Tetrameric Potassium Ion Channel KcsA. *Journal of the American Chemical Society* **131**, 15246-15250.
43. Pliotas, C., Ward, R., Branigan, E., Rasmussen, A., Hagelueken, G., Huang, H. X., Black, S. S., Booth, I. R., Schiemann, O. & Naismith, J. H. (2012). Conformational state of the MscS mechanosensitive channel in solution revealed by pulsed electron-electron double resonance (PELDOR) spectroscopy. *Proc Natl Acad Sci U S A* **109**, E2675-E2682.
  44. Dellisanti, C. D., Ghosh, B., Hanson, S. M., Raspanti, J. M., Grant, V. A., Diarra, G. M., Schuh, A. M., Satyshur, K., Klug, C. S. & Czajkowski, C. (2013). Site-directed spin labeling reveals pentameric ligand-gated ion channel gating motions. *PLoS Biol* **11**, e1001714.
  45. Georgieva, E. R., Borbat, P. P., Norman, H. D. & Freed, J. H. (2015). Mechanism of influenza A M2 transmembrane domain assembly in lipid membranes. *Scientific Reports* **5**, 11757.
  46. Hilger, D., Jung, H., Padan, E., Wegener, C., Vogel, K.-P., Steinhoff, H.-J. & Jeschke, G. (2005). Assessing Oligomerization of Membrane Proteins by Four-Pulse DEER: pH-Dependent Dimerization of NhaA Na<sup>+</sup>/H<sup>+</sup> Antiporter of *E. coli*. *Biophysical Journal* **89**, 1328-1338.
  47. Hagelueken, G., Ingledew, W. J., Huang, H., Petrovic-Stojanovska, B., Whitfield, C., ElMkami, H., Schiemann, O. & Naismith, J. H. (2009). PELDOR Spectroscopy Distance Fingerprinting of the Octameric Outer-Membrane Protein Wza from *Escherichia coli*. *Angewandte Chemie-International Edition* **48**, 2904-2906.

48. Rodriguez, F., Rouse, S. L., Tait, C. E., Harmer, J., De Riso, A., Timmel, C. R., Sansom, M. S., Berks, B. C. & Schnell, J. R. (2013). Structural model for the protein-translocating element of the twin-arginine transport system. *Proc Natl Acad Sci U S A* **110**, E1092-101.
49. Edwards, D. T., Huber, T., Hussain, S., Stone, K. M., Kinnebrew, M., Kaminker, I., Matalon, E., Sherwin, M. S., Goldfarb, D. & Han, S. (2014). Determining the Oligomeric Structure of Proteorhodopsin by  $Gd^{3+}$ -Based Pulsed Dipolar Spectroscopy of Multiple Distances. *Structure* **22**, 1677-1686.
50. Traaseth, N. J., Verardi, R., Torgersen, K. D., Karim, C. B., Thomas, D. D. & Veglia, G. (2007). Spectroscopic validation of the pentameric structure of phospholamban. *Proc Natl Acad Sci U S A* **104**, 14676-81.
51. Giannoulis, A., Ward, R., Branigan, E., Naismith, J. H. & Bode, B. E. (2013). PELDOR in rotationally symmetric homo-oligomers. *Molecular Physics* **111**, 2845-2854.
52. von Hagens, T., Polyhach, Y., Sajid, M., Godt, A. & Jeschke, G. (2013). Suppression of ghost distances in multiple-spin double electron-electron resonance. *Phys Chem Chem Phys* **15**, 5854-66.
53. Valera, S., Ackermann, K., Pliotas, C., Huang, H. X., Naismith, J. H. & Bode, B. E. (2016). Accurate Extraction of Nanometer Distances in Multimers by Pulse EPR. *Chemistry-a European Journal* **22**, 4700-4703.
54. Jeschke, G. (2013). Conformational dynamics and distribution of nitroxide spin labels. *Progress in Nuclear Magnetic Resonance Spectroscopy* **72**, 42-60.
55. Wang, X., Lee, H. W., Liu, Y. Z. & Prestegard, J. H. (2011). Structural NMR of protein oligomers using hybrid methods. *Journal of Structural Biology* **173**, 515-529.

56. Yang, Y. H., Ramelot, T. A., McCarrick, R. M., Ni, S. S., Feldmann, E. A., Cort, J. R., Wang, H. A., Ciccocanti, C., Jiang, M., Janjua, H., Acton, T. B., Xiao, R., Everett, J. K., Montelione, G. T. & Kennedy, M. A. (2010). Combining NMR and EPR Methods for Homodimer Protein Structure Determination. *Journal of the American Chemical Society* **132**, 11910-11913.
57. Jung, K. H., Trivedi, V. D. & Spudich, J. L. (2003). Demonstration of a sensory rhodopsin in eubacteria. *Molecular Microbiology* **47**, 1513-1522.
58. Sineshchekov, O. A., Trivedi, V. D., Sasaki, J. & Spudich, J. L. (2005). Photochromicity of Anabaena sensory rhodopsin, an atypical microbial receptor with a cis-retinal light-adapted form. *J Biol Chem* **280**, 14663-8.
59. Ward, M. E., Wang, S., Munro, R., Ritz, E., Hung, I., Gor'kov, P. L., Jiang, Y., Liang, H., Brown, L. S. & Ladizhansky, V. (2015). In Situ Structural Studies of Anabaena Sensory Rhodopsin in the *E. coli* Membrane. *Biophysical Journal* **108**, 1683-1696.
60. Wang, S., Munro, R. A., Shi, L., Kawamura, I., Okitsu, T., Wada, A., Kim, S. Y., Jung, K. H., Brown, L. S. & Ladizhansky, V. (2013). Solid-state NMR spectroscopy structure determination of a lipid-embedded heptahelical membrane protein. *Nature Methods* **10**, 1007-12.
61. Vogeley, L., Sineshchekov, O. A., Trivedi, V. D., Sasaki, J., Spudich, J. L. & Luecke, H. (2004). Anabaena sensory rhodopsin: A photochromic color 0 sensor at 2.0 angstrom. *Science* **306**, 1390-1393.
62. Ward, M. E., Wang, S., Krishnamurthy, S., Hutchins, H., Fey, M., Brown, L. S. & Ladizhansky, V. (2014). High-resolution paramagnetically enhanced solid-state NMR

- spectroscopy of membrane proteins at fast magic angle spinning. *J Biomol NMR* **58**, 37-47.
63. Alaouie, A. M. & Smirnov, A. I. (2005). Cooperativity and kinetics of phase transitions in nanopore-confined bilayers studied by differential scanning calorimetry. *Biophysical Journal* **88**, L11-L13.
64. Nogly, P., James, D., Wang, D. J., White, T. A., Zatsepin, N., Shilova, A., Nelson, G., Liu, H. G., Johansson, L., Heymann, M., Jaeger, K., Metz, M., Wickstrand, C., Wu, W. T., Bath, P., Berntsen, P., Oberthuer, D., Panneels, V., Cherezov, V., Chapman, H., Schertler, G., Neutze, R., Spence, J., Moraes, I., Burghammer, M., Standfuss, J. & Weierstall, U. (2015). Lipidic cubic phase serial millisecond crystallography using synchrotron radiation. *Iucrj* **2**, 168-176.
65. Matthews, J. M. & Sunde, M. (2012). Dimers, oligomers, everywhere. *Adv Exp Med Biol* **747**, 1-18.
66. Shi, L., Kawamura, I., Jung, K. H., Brown, L. S. & Ladizhansky, V. (2011). Conformation of a seven-helical transmembrane photosensor in the lipid environment. *Angew Chem Int Ed Engl* **50**, 1302-5.
67. Wang, S., Shi, L., Okitsu, T., Wada, A., Brown, L. S. & Ladizhansky, V. (2012). Solid-state NMR  $^{13}\text{C}$  and  $^{15}\text{N}$  resonance assignments of a seven-transmembrane helical protein *Anabaena* Sensory Rhodopsin. *Biomol NMR Assign.* **7**, 253-256.
68. Kondoh, M., Inoue, K., Sasaki, J., Spudich, J. L. & Terazima, M. (2011). Transient dissociation of the transducer protein from *Anabaena* sensory rhodopsin concomitant with formation of the M state produced upon photoactivation. *J Am Chem Soc* **133**, 13406-12.

69. Sasaki, T., Kubo, M., Kikukawa, T., Kamiya, M., Aizawa, T., Kawano, K., Kamo, N. & Demura, M. (2009). Halorhodopsin from *natronomonas pharaonis* forms a trimer even in the presence of a detergent, dodecyl-beta-D-maltoside. *Photochem Photobiol* **85**, 130-6.
70. Ward, M. E., Ritz, E., Ahmed, M. A. M., Bamm, V. V., Harauz, G., Brown, L. S. & Ladizhansky, V. (2015). Proton detection for signal enhancement in solid-state NMR experiments on mobile species in membrane proteins. *Journal of Biomolecular NMR* **63**, 375-388.
71. Marko, A. & Prisner, T. F. (2013). An algorithm to analyze PELDOR data of rigid spin label pairs. *Physical Chemistry Chemical Physics* **15**, 619-627.
72. Milov, A. D., Tsvetkov, Y. D., Formaggio, F., Crisma, M., Toniolo, C. & Raap, J. (2000). Self-assembling properties of membrane-modifying peptides studied by PELDOR and CW-ESR spectroscopies. *Journal of the American Chemical Society* **122**, 3843-3848.
73. Shen, Y., Delaglio, F., Cornilescu, G. & Bax, A. (2009). TALOS+: a hybrid method for predicting protein backbone torsion angles from NMR chemical shifts. *J Biomol NMR* **44**, 213-23.
74. Jeschke, G., Chechik, V., Ionita, P., Godt, A., Zimmermann, H., Banham, J., Timmel, C. R., Hilger, D. & Jung, H. (2006). DeerAnalysis2006 - a comprehensive software package for analyzing pulsed ELDOR data. *Applied Magnetic Resonance* **30**, 473-498.
75. Dalmas, O., Hyde, H. C., Hulse, R. E. & Perozo, E. (2012). Symmetry-Constrained Analysis of Pulsed Double Electron-Electron Resonance (DEER) Spectroscopy Reveals the Dynamic Nature of the KcsA Activation Gate. *Journal of the American Chemical Society* **134**, 16360-16369.

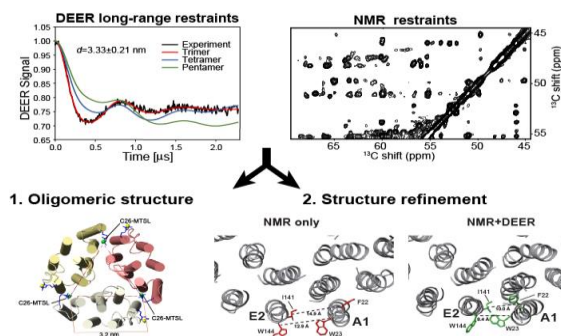
76. Dominguez, C., Boelens, R. & Bonvin, A. M. (2003). HADDOCK: a protein-protein docking approach based on biochemical or biophysical information. *J Am Chem Soc* **125**, 1731-7.
77. de Vries, S. J., van Dijk, A. D., Krzeminski, M., van Dijk, M., Thureau, A., Hsu, V., Wassenaar, T. & Bonvin, A. M. (2007). HADDOCK versus HADDOCK: new features and performance of HADDOCK2.0 on the CAPRI targets. *Proteins* **69**, 726-33.
78. Kucerka, N., Kiselev, M. A. & Balgavy, P. (2004). Determination of bilayer thickness and lipid surface area in unilamellar dimyristoylphosphatidylcholine vesicles from small-angle neutron scattering curves: a comparison of evaluation methods. *Eur Biophys J* **33**, 328-34.
79. Borbat, P. P. & Freed, J. H. (2014). Pulse Dipolar Electron Spin Resonance: Distance Measurements. In *Structural Information from Spin-Labels and Intrinsic Paramagnetic Centres in the Biosciences* (Timmel, C. R. & Harmer, J. R., eds.), Vol. 152, pp. 1-82.
80. Bhatnagar, J., Borbat, P. P., Pollard, A. M., Bilwes, A. M., Freed, J. H. & Crane, B. R. (2010). Structure of the Ternary Complex Formed by a Chemotaxis Receptor Signaling Domain, the CheA Histidine Kinase, and the Coupling Protein CheW As Determined by Pulsed Dipolar ESR Spectroscopy. *Biochemistry* **49**, 3824-3841.
81. Janzen, E. G., Stronks, H. J., Dubose, C. M., Poyer, J. L. & McCay, P. B. (1985). Chemistry and biology of spin-trapping radicals associated with halocarbon metabolism in vitro and in vivo. *Environmental Health Perspectives* **64**, 151-170.
82. Zhang, R. L., Hirsch, O., Mohsen, M. & Samuni, A. (1994). Effects of Nitroxide Stable Radicals on Juglone Cytotoxicity. *Archives of Biochemistry and Biophysics* **312**, 385-391.

83. BeitYannai, E., Zhang, R. L., Trembovler, V., Samuni, A. & Shohami, E. (1996). Cerebroprotective effect of stable nitroxide radicals in closed head injury in the rat. *Brain Research* **717**, 22-28.
84. Samuni, A., Goldstein, S., Russo, A., Mitchell, J. B., Krishna, M. C. & Neta, P. (2002). Kinetics and mechanism of hydroxyl radical and OH-adduct radical reactions with nitroxides and with their hydroxylamines. *Journal of the American Chemical Society* **124**, 8719-8724.
85. Morse, P. D. & Smirnov, A. I. (1995). Simultaneous ESR measurements of the kinetics of oxygen consumption and spin label reduction by mammalian cells. *Magnetic Resonance in Chemistry* **33**, S46-S52.
86. Brunger, A. T., Adams, P. D., Clore, G. M., DeLano, W. L., Gros, P., Grosse-Kunstleve, R. W., Jiang, J. S., Kuszewski, J., Nilges, M., Pannu, N. S., Read, R. J., Rice, L. M., Simonson, T. & Warren, G. L. (1998). Crystallography & NMR system: A new software suite for macromolecular structure determination. *Acta Crystallogr D Biol Crystallogr* **54**, 905-21.
87. Sammalkorpi, M. & Lazaridis, T. (2007). Modeling a spin-labeled fusion peptide in a membrane: implications for the interpretation of EPR experiments. *Biophys J* **92**, 10-22.
88. Klare, J. P., Bordignon, E., Engelhard, M. & Steinhoff, H. J. (2004). Sensory rhodopsin II and bacteriorhodopsin: Light activated helix F movement. *Photochemical & Photobiological Sciences* **3**, 543-547.
89. Krause, N., Engelhard, C., Heberle, J., Schlesinger, R. & Bittl, R. (2013). Structural differences between the closed and open states of channelrhodopsin-2 as observed by EPR spectroscopy. *Febs Letters* **587**, 3309-3313.



90. Sattig, T., Rickert, C., Bamberg, E., Steinhoff, H. J. & Bamann, C. (2013). Light-Induced Movement of the Transmembrane HelixB in Channelrhodopsin-2. *Angewandte Chemie-International Edition* **52**, 9705-9708.
91. Wada, Y., Kawanabe, A., Furutani, Y., Kandori, H. & Ohtani, H. (2008). Quantum yields for the light adaptations in Anabaena sensory rhodopsin and bacteriorhodopsin. *Chemical Physics Letters* **453**, 105-108.
92. Cornish, V. W., Benson, D. R., Altenbach, C. A., Hideg, K., Hubbell, W. L. & Schultz, P. G. (1994). Site-specific incorporation of biophysical probes into proteins. *Proc Natl Acad Sci U S A* **91**, 2910-4.
93. Gross, A., Columbus, L., Hideg, K., Altenbach, C. & Hubbell, W. L. (1999). Structure of the KcsA potassium channel from Streptomyces lividans: A site-directed spin labeling study of the second transmembrane segment. *Biochemistry* **38**, 10324-10335.
94. Religa, T. L., Ruschak, A. M., Rosenzweig, R. & Kay, L. E. (2011). Site-directed methyl group labeling as an NMR probe of structure and dynamics in supramolecular protein systems: applications to the proteasome and to the ClpP protease. *J Am Chem Soc* **133**, 9063-8.
95. daCosta, C. J. & Baenziger, J. E. (2003). A rapid method for assessing lipid:protein and detergent:protein ratios in membrane-protein crystallization. *Acta Crystallogr D Biol Crystallogr* **59**, 77-83.
96. Fung, B. M., Khitritin, A. K. & Ermolaev, K. (2000). An improved broadband decoupling sequence for liquid crystals and solids. *J. Magn. Reson.* **142**, 97-101.
97. Hartmann, S. R. & Hahn, E. L. (1962). Nuclear double resonance in the rotating frame. *Phys. Rev.* **128**, 2042-2053.

98. Baldus, M., Petkova, A. T., Herzfeld, J. & Griffin, R. G. (1998). Cross polarization in the tilted frame: assignment and spectral simplification in heteronuclear spin systems. *Molecular Physics* **95**, 1197-1207.
99. Delaglio, F., Grzesiek, S., Vuister, G. W., Zhu, G., Pfeifer, J. & Bax, A. (1995). NMRPipe: a multidimensional spectral processing system based on UNIX pipes. *J. Biomol. NMR* **6**, 277-293.
100. Morcombe, C. R. & Zilm, K. W. (2003). Chemical shift referencing in MAS solid state NMR. *Journal of Magnetic Resonance* **162**, 479-486.
101. Goddard, T. D. & Kneller, D. G. SPARKY 3, University of California, San Francisco. In <https://www.cgl.ucsf.edu/home/sparky/>.
102. Pannier, M., Veit, S., Godt, A., Jeschke, G. & Spiess, H. W. (2000). Dead-Time Free Measurement of Dipole–Dipole Interactions between Electron Spins. *Journal of Magnetic Resonance* **142**, 331-340.



## Graphical abstract

## Highlights

- Lipid-embedded oligomeric proteins are not readily amenable to structural methods
- DEER and ssNMR employ the same preparation protocol of membrane protein samples
- Geometry of ASR oligomers are derived from the analysis of a multi-spin DEER signal
- Significant refinement of ASR ssNMR structure is achieved by adding DEER constraints
- Combined DEER+ssNMR can determine structures of membrane protein assemblies